Chemical Science

Accepted Manuscript

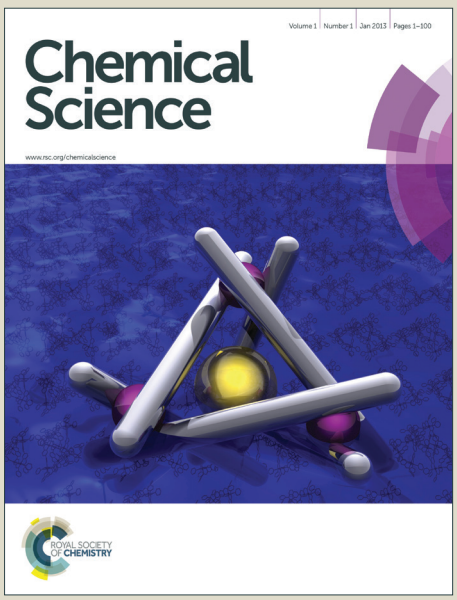

ROYAL SOCIETY OF CHEMISTRY

www.rsc.org/chemicalscience

Cite this: DOI: 10.1039/c0xx00000x

www.rsc.org/xxxxxx

ARTICLE TYPE

In situ activating and monitoring the evolution of intracellular caspase family†

Lei Zhang, Jianping Lei*, Jintong Liu, Fengjiao Ma and Huangxian Ju*

Received (in XXX, XXX) XthXXXXXXXXX 20XX, Accepted Xth XXXXXXXXX 20XX

DOI: 10.1039/c000000x

The evolution of intracellular caspase family is crucial in cell apoptosis. To evaluate this process, a universal platform of *in situ* activating and monitoring the evolution of intracellular caspase is designed. Using well-known gold nanostructure as a model of both nanocarrier and matter inducing the cell apoptosis for photothermal therapy, a nanoprobe is prepared by assembly of two kinds of dye-labelled peptides specific to upstream caspase-9 and downstream caspase-3 as the signal switch and folic acid as a targeting moiety. The energy transfer from dyes to the gold nanocarrier at two surface plasmon resonance absorption wavelengths leads to their fluorescence quenching. Upon endocytosis of the nanoprobe to perform the thearapy agnasit cancer cells, the peptides are successively cleaved by intracellular caspase activation with the evolution from upstream to downstream, which lights up the fluorescence of the dyes sequentially, and can be used to quantify both caspase-9 and caspase-3 activities in cancer cells and to monitor their evolution in living mice. The recovered fluorescence could also be used to assesse the therapeutic efficiency. This work provides a novel powerful tool for studying the evolution of intracellular caspase family and elucidating the biological roles of caspases in cancer cell apoptosis.

Introduction

Caspases are a family of cysteine-aspartic proteases that are only activated during cell apoptosis, and can be used as feedback markers of cell death.[1] Caspase-controlled apoptosis has a characteristic enzyme cascade, which involves multiple caspases at different stages and pathways.[2] Upstream caspase, such as caspase-9 (casp-9), plays a central role in the induction of apoptosis, while downstream caspase such as caspase-3 (casp-3) is critical for carrying out the final step of cell apoptosis. Thus the evaluation of intracellular caspase family is essential to elucidate the cell apoptosis process. Indeed, many fluorescent probes have been developed for imaging of caspase activity in living cells and animals,[3] and real-time monitoring of caspase cascade activation by diverse pairs of dyes and corresponding quenchers.[4] However, besides the sensing probes, some additional inducers are usually needed to activate intracellular caspase activity.[4,5] Thus an apoptosis sensor has developed for *in situ* activation and imaging of intracellular casp-3 using aggregation-induced emission.[6] The platform for *in situ* activating and monitoring the evolution of caspase family during cell apoptosis is still an urgent need.

State Key Laboratory of Analytical Chemistry for Life Science, School of Chemistry and Chemical Engineering, Nanjing University, Nanjing 210093, P. R. China. Fax: +86(25) 83593593; Tel: +86(25) 83593593; E-mail: jpl@nju.edu.cn, hxju@nju.edu.cn.

† Electronic Supplementary Information (ESI) available: Experimental details and supplementary figures. See DOI: 10.1039/c000000x/.

Noble metal nanostructures with good biocompatibility have received considerable research interest due to their strong absorption in near-infrared (NIR) region and high photothermal conversion efficiency.[7] Herein, using gold nanorod (AuNR) as the model of both nanocarrier and matter inducing the cell apoptosis, which was found to be able to simultaneously quench two kinds of dyes at two unique surface plasmon resonance (SPR) absorption wavelengths, a versatile nanoprobe was designed for *in situ* activating and monitoring the evolution of caspase family from upstream to downstream via NIR photothermal treatment.

The nanoprobe was prepared by assembling fluorescein isothiocyanate (FITC)-labelled peptide specific to casp-9 (peptide-9) and cyanine-5.5 (Cy5.5)-labelled peptide specific to casp-3 (peptide-3) as signal switches and recognition elements, and folic acid (FA) as a target specific moiety on AuNR (Scheme 1). Their fluorescence was initially quenched via energy transfer from FITC and Cy5.5 to AuNR with transverse and longitudinal SPR absorption, respectively. Upon endocytosis of the nanoprobe and NIR irradiation, cell apoptosis was encouraged by the photothermal effect and thus the peptide could be cleaved successively by corresponding activated caspase from upstream casp-9 to downstream casp-3, which released the dyes from the nanocarrier for fluorescent imaging. The turn-on signals provided an efficient way for quantification of both caspa-9 and casp-3 activities in cancer cells and monitoring of their evolution in living mice. Since caspase activity is the marker of cell apoptosis, the fluorescence response could also be used to monitor the therapeutic efficacy in real time.

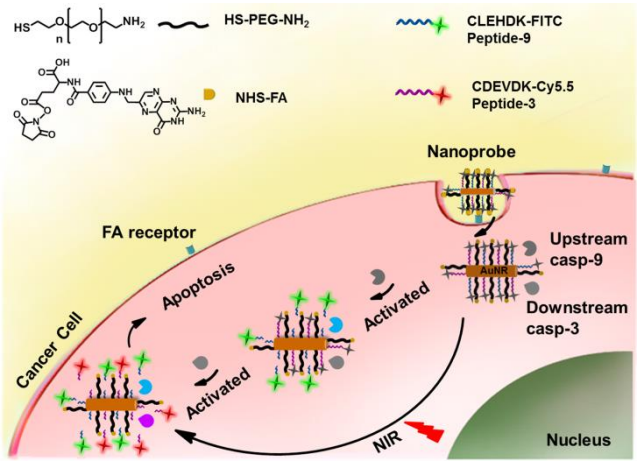

Scheme 1 Schematic illustration of an integrated platform for *in situ* monitoring the evolution of caspase family activated via real-time NIR photothermal therapy.

Results and discussion

Characterizations of the nanoprobe

Gold nanocarrier was synthesized according to the typical method of seed-mediated growth and well characterized (see ESI, Fig. S1A and S2†).[8] For efficient preparation of the nanoprobe, HS-poly(ethylene glycol)-NH_2 was used to protect the nanorod from aggregation and efficiently bind N-hydroxysuccinimide (NHS)-functionalized FA via a typical amide reaction (see ESI, Fig. S3†).[9] After functionalization with dye-labelled peptides and PEG, a slight red shift of the characteristic absorption at 787 nm was observed in the UV-vis spectra (Fig. S2A†), while the binding of NHS-FA to the PEG produced a characteristic absorption peak of FA at 280 nm.[10] The functionalization did not change their surface profile (Fig. S1B†). In addition, compared with raw nanorod, the nanoprobe showed an Au-Br Raman peak with the shift from 180 cm^{-1} to 261 cm^{-1} (Fig. S2B†), and the surface changed to a negative ζ potential (Fig. S2C†). These results indicated that the nanoprobe was successfully synthesized with good-dispersibility and excellent optical properties for the fluorescent detection and imaging.

In vitro detection of casp-9 and casp-3 activities

To test the validity of the nanoprobe to caspase, *in vitro* enzymatic assays were performed with recombinant caspase proteins. Since the emission of FITC and Cy5.5 overlapped with the transverse and longitudinal SPR absorption of the gold nanorod (see ESI, Fig. S4†), their fluorescence (FL) was quenched via FRET (see ESI, Fig. S5†), respectively. After incubating the mixture of the nanoprobe and recombinant caspase proteins in caspase assay buffer at 37 ℃, the FL was significantly enhanced at 517 and 694 nm, respectively, indicating that the enzymatic reaction released the dyes from the gold nanostructure, which could be inhibited by the specific inhibitors of casp-9 or casp-3 (Fig. 1A). At the optimized reaction time of 80 min (Fig. 1B), the FL intensity linearly increased with the enhancive concentration of caspase (Fig. 1C and 1D). The cleavage reaction showed good specificity to caspase against other interferents (Fig. 1E and 1F), leading to a method for detection of caspase activity.

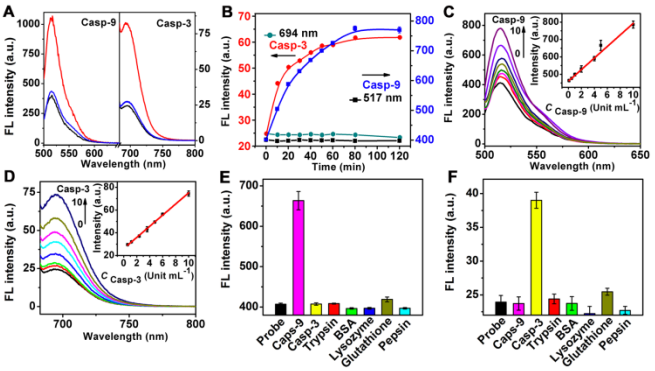

Fig. 1 (A) Fluorescence spectra of nanoprobe ($OD_{787\,nm}$ = 0.5, black) and its mixtures with casp-9 or casp-3 (20 Unit mL^{-1}) in the absence (red) and presence (blue) of casp-9 or casp-3 inhibitor (10 μM). (B) Time-dependent fluorescence responses of nanoprobe (10 μL) in the absence (black) and presence (blue) of casp-9 (8.0 Unit mL^{-1}) at 517 nm, and in the absence (green) and presence (red) of casp-3 (8.0 Unit mL^{-1}) at 694 nm. (C, D) Fluorescence spectra of nanoprobe (10 μL) after incubation with (C) 0, 0.1, 0.5, 1.0, 2.0, 4.0, 5.0 and 10 Unit mL^{-1} casp-9 and (D) 0, 0.6, 1.2, 2.4, 3.6, 4.8, 6.0 and 10 Unit mL^{-1} casp-3 for 80 min. Insets: plots of FL intensity *vs.* casp-9 and casp-3 concentration. Fluorescent response of nanoprobe at (E) 517 and (F) 694 nm to casp-9 (5.0 Unit mL^{-1}), casp-3 (5.0 Unit mL^{-1}), glutathione (1.0 mM) and other proteins (1.0 μM).

The amounts of peptide-9 and peptide-3 loaded on the nanocarrier were determined to be 1.01×10^4 and 9.73×10^3, respectively (see ESI, Fig. S6†). The kinetic analysis of cleavage reactions was carried out by incubating casp-9 or casp-3 with the increasing concentration of nanoprobe at 37 ℃. The Michaelis constants, K_M, of casp-9 and casp-3 were calculated to be 6.70 ± 0.4 and 5.58 ± 0.3 μM, and the kinetic constants, k_{cat}, were 1.69 and 1.62 s^{-1}, respectively (Fig. 2A-2D). The k_{cat} value for casp-3 was comparable to the value reported with another fluorescent probe,[11] and the K_M value was lower than 12.7 μM of a commercial substrate for casp-3,[12] indicating the better affinity between the nanoprobe and caspase.

Owing to the essential roles of caspases in cell apoptosis, the selectivity of nanoprobe in monitoring the activity of caspase in complex cellular samples was examined. HeLa cell lysates were

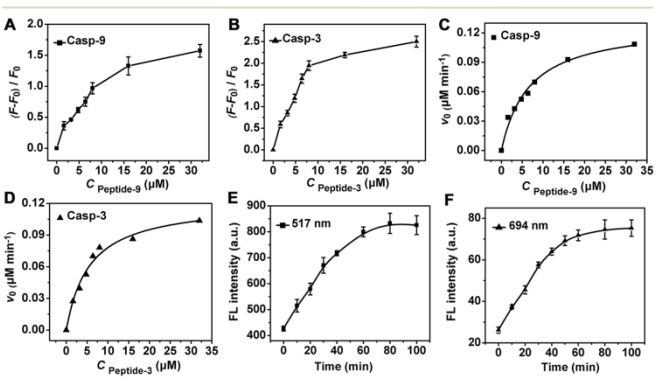

Fig. 2 Plots of $(F-F_0)/F_0$ *vs.* concentrations of (A) peptide-9 and (B) peptide-3 loaded on nanoprobe, where F_0 and F are the fluorescence intensity of nanoprobe and the mixture of nanoprobe with target caspase (10 Unit mL^{-1}) after incubation for 80 min at 37 ℃, respectively. Caspase enzymatic kinetics assay of (C) casp-9 (10 Unit mL^{-1}) and (D) casp-3 (10 Unit mL^{-1}) with an increasing of substrate concentration. Time-dependence of the fluorescent response of nanoprobe (10 μL) in apoptotic HeLa cell lysate at (E) 517 nm and (F) 694 nm.

collected after treatment with a commonly used cell apoptosis inducer (staurosporine, 2 μM) to activate the caspase. Time-dependent fluorescence at both 517 and 694 nm with the excitation wavelengths of 490 and 675 nm was detected during the incubation of the lysate with nanoprobe, respectively (Fig. 2E and 2F), which showed acceptable selectivity of the nanoprobe for intracellular activated casp-9 and casp-3.

Monitoring the evolution of intracellular caspase family

Prior to intracellular usage, the cytotoxicity of nanoprobe and NIR irradiation (808 nm) was examined with MTT assay (see ESI, Fig. S7†). After incubated with different amounts of nanoprobe for 3 h or treated with NIR for 50 min, HeLa cells still maintained a high viability, indicating good biocompatibility of nanoprobe and low cytotoxicity of NIR irradiation itself. Compared with HaCat normal cells, the nanoprobe transfected HeLa cells showed obvious apoptosis after NIR irradiation at 4 W cm^{-2} for 10 min. The nanoprobe could enter HeLa cells via FA receptor-mediated endocytosis and accumulate in the cytoplasm out of cell nucleus (see ESI, Figs. S8 and S9†), which was also verified by TEM image (see ESI, Fig. S10†). The weak fluorescence of FITC could be observed in MCF-7 and HeLa cells, while no change was observed in A549 cells, confirming FA receptor-mediated internalization of nanoprobe.

To employ the probe for monitoring the evolution of caspase family from upstream to downstream during therapy, HeLa cells were seeded in a confocal dish for 24 h. After incubation with nanoprobe for 3 h and then treatment with NIR irradiation for different times, HeLa cells were then performed for confocal fluorescence imaging (Fig. 3). Little fluorescence was observed in the nanoprobe transfected HeLa cells before NIR irradiation. After NIR irradiation for 3 min, the fluorescence of FITC (green) in HeLa cells was firstly lighted up and increased gradually with the progress of cell apoptosis induced by the photothermal effect of the gold nanocarrier, while the fluorescence of Cy5.5 (red) was observed after NIR irradiation for 10 min, indicating that casp-9 was activated in the initial stage of cell apoptosis, which thus played the role of initiator in the caspase family. With the deepening of cell apoptosis degree, casp-3 was activated to show the fluorescence of Cy5.5. After the irradiation for 30 min,

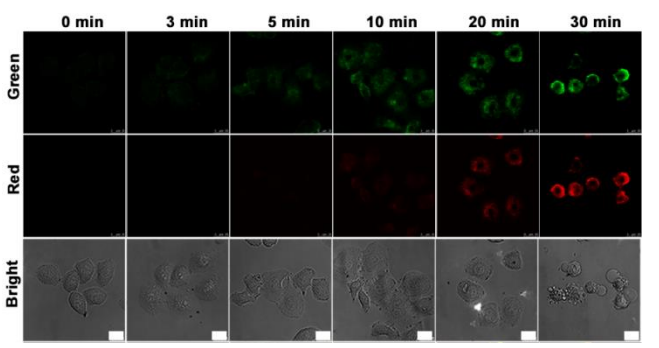

Fig. 3 Confocal fluorescence images of HeLa cells incubated with the nanoprobe (10 μL, $OD_{787\ nm}$ = 0.5) for 3 h and then treated with NIR irradiation at 4 W cm^{-2} for different times. Green fluorescence at $\lambda_{ex/em}$ of 488/500–560 nm. Red fluorescence at $\lambda_{ex/em}$ of 633/680–740 nm. Scale bars, 25 μm.

apoptotic HeLa cells showed shrinkage with maximum fluorescence intensity at both green and red channel.

The initiator role of casp-9 in the evolution of caspase family could be confirmed with the inhibitor treatment (Fig. 4). After the probe transfected HeLa cells were treated with casp-3 inhibitor, they showed the green fluorescence of FITC, and the red Cy5.5 disappeared, indicating the effective inhibition of the inhibitor to casp-3, which did not affect the activation of casp-9 to release FITC from the nanoprobe. Contrarily, after the probe transfected HeLa cells were treated with casp-9 inhibitor, both the green fluorescence and the followed red fluorescence disappeared. Thus the activation of casp-3 depended on casp-9, which demonstrated the mitochondrial-involvement apoptotic pathway.[13] The evolution was also validated by flow cytometric assays, which showed the increasing fluorescence of FITC and Cy5.5 (Fig. 5A) as the raised apoptosis percentage (Fig. 5B).

The mitochondrial pathway of apoptosis was confirmed using Rhodamine 123 staining with green fluorescence (see ESI, Fig. S11†), which is readily sequestered by living mitochondria in cells undergoing apoptosis.[14] Furthermore, both apoptotic detection kit with flow cytometry (Fig. 5B) and fluorescence imaging of HeLa cells stained with 4',6-diamidino-2-phenylindole (DAPI) dye special for cell nucleus (see ESI, Fig. S12†) verified the caspase-dependent early apoptosis through mitochondrial pathway.[15]

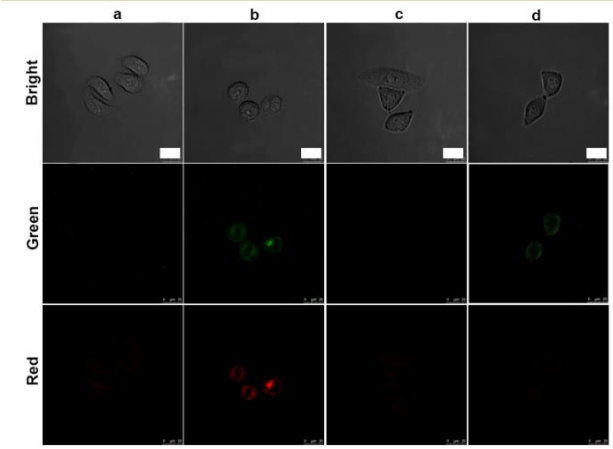

Fig. 4 Confocal fluorescence images of HeLa cells incubated with 10 μL nanoprobe (a) before and (b) after NIR irradiation for 20 min, and treated with (c) casp-9 and (d) casp-3 inhibitor for 6 h and then NIR irradiation for 20 min. Green fluorescence at $\lambda_{ex/em}$ of 488/500–560 nm. Red fluorescence at $\lambda_{ex/em}$ of 633/680–740 nm. Scale bars, 25 μm.

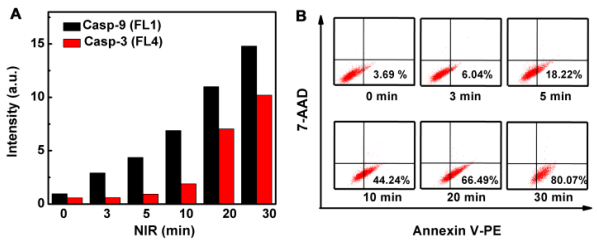

Fig. 5 (A) Flow cytometric detection of HeLa cells after incubation with the nanoprobe (50 μL, $OD_{787\ nm}$ = 0.5) for 3 h and then NIR irradiation for different times. (B) Flow cytometric analysis of the same treated HeLa cells using apoptosis kit with the dual fluorescence of Annexin V-PE/7-AAD.

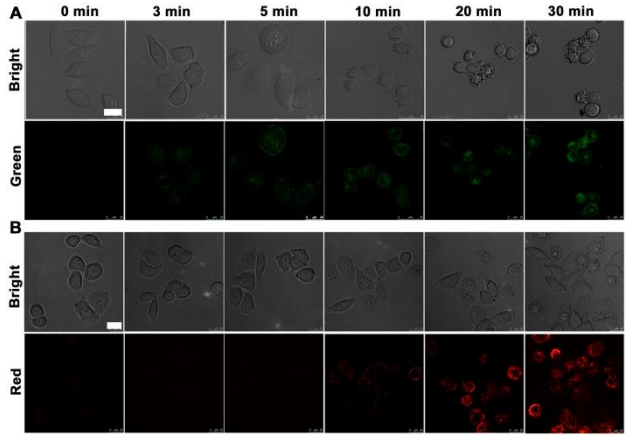

Fig. 6 Confocal fluorescence images of HeLa cells after incubation with (A) nanoprobe-9 (10 μL) and (B) nanoprobe-3 (10 μL) for 3 h and then NIR irradiation for different times. Green fluorescence at $\lambda_{ex/em}$ of 488/500–560 nm. Red fluorescence at $\lambda_{ex/em}$ of 633/680–740 nm. Scale bars, 25 μm.

For further verifying the application of the designed nanoprobe in monitoring the evolution of caspase family, nanoprobe-9 and nanoprobe-3 were also synthesized (see ESI). After incubating HeLa cells with these probes for 3 h at 37 ℃, the cells were treated with NIR irradiation for different times. Consistent with the appearance shown in Fig. 3, the nanoprobe-9 transfected HeLa cells showed the green fluorescence at 3 min postirradiation followed with casp-9 activation (Fig. 6A), while the nanoprobe-3 transfected cells showed red fluorescence from 10 min due to the activation of casp-3 (Fig. 6B). The specificity of intracellular cleavage reaction was demonstrated by immunofluorescence imaging (see ESI, Fig. S13†). The excellent overlap was observed both between the green fluorescence of nanoprobe-9 and red immunofluorescence signal of casp-9 and between the red fluorescence of nanoprobe-3 and green immunofluorescence signal of casp-3, suggesting intracellular caspase-specific activation and imaging.

Quantifications of two intracellular caspases

The proposed probe could be used to quantify the activities of two intracellular caspases. To obtain the calibration curve, HeLa cells (5.0×10^4) were incubated with nanoprobe for 3 h and then treated with NIR irradiation with increasing time to obtain the confocal fluorescence images. The FL intensity was measured in the cell area with Leica software (Fig. 7A-7C). The corresponding casp-9 and casp-3 activities of the treated HeLa cells were detected via *in vitro* casp-9 and casp-3 kit analysis of the cell extracts using their standard curves (Fig. 7D-7G). The obtained caspase activities (*c*) were then used for obtaining the calibration curve for quantification of casp-9 and casp-3 activities in single cell from the FL intensity (Fig. 7H and 7I). The plots of FL intensity (*FI*) *vs.* *c* (10^{-7} Unit) in single cell followed the linear regression equations of $FI = 5.67 + 2.10 \times c$ for casp-9 and $FI = 5.33 + 2.33 \times c$ for casp-3. The average activity of casp-9 and casp-3 in a single HeLa was cell was 4.25 and 5.09 $\times 10^{-7}$ Unit after the therapy-inducing apoptosis. Therefore, the proposed strategy possessed the applicability for monitoring the change of intracellular caspase activity.

Evaluatation of therapeutic efficiency in real-time

Interesting, the unique caspase-responsive fluorescence of nanoprobe could be used to evaluate the therapeutic efficiency. To verify this capability, the fluorescent (FITC and Cy5.5) and morphologic changes of nanoprobe transfected HeLa cells were tracked in real time under NIR irradiation by confocal fluorescence imaging (see ESI, Fig. S14†, Fig. 8), which showed the increasing luminescence with the cell apoptosis. This result proved that the functionalized nanoprobe not only had the potential for *in situ* activation and detection of intracellular caspase, but also could be used for real-time monitoring the therapeutic effect of targeted-cancer cell, providing a novel tool to evaluate the therapeutic responses.

Monitoring caspase activity in living mouse

This design could also be applied to monitor caspase activity in living mouse activated by the treatment effect of the gold nanostructure. HeLa tumor was subcutaneously implanted on the flank of the nude mice. The tumor-bearing mice were then intravenously injected with nanoprobe. At 24-h postinjection, tumor accumulation of the nanoprobe was found to be highly efficient (see ESI, Fig. S15†). Afterward, the mice were irradiated with a NIR laser for 30 min to perform the therapy. The therapeutic efficiency was assessed by monitoring the tumor volume after treatment, which showed that the tumor growth was

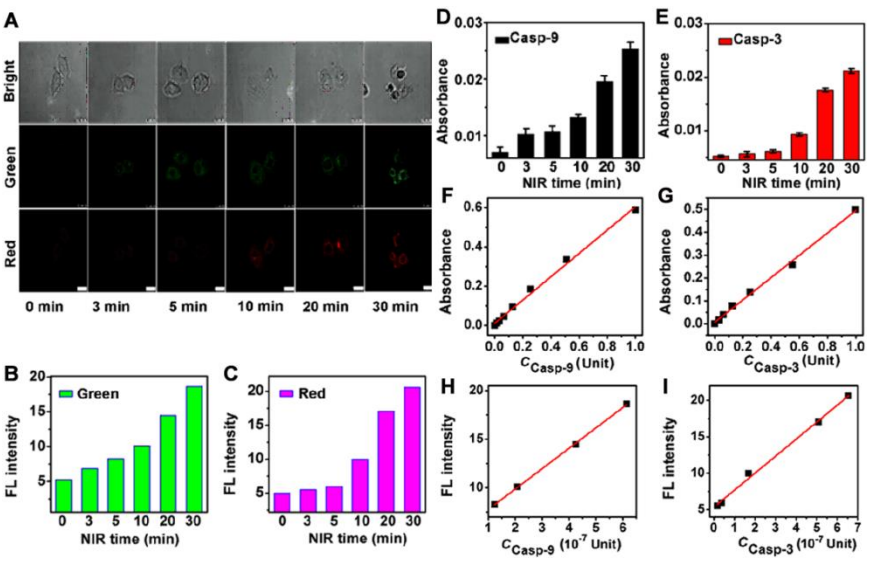

Fig. 7 (A) Confocal fluorescence images of HeLa cells treated with 10 μL nanoprobe ($OD_{787\,nm}$ = 0.5) for 3 h and then NIR irradiation for different times. Green fluorescence at $\lambda_{ex/em}$ of 488/500–560 nm; red fluorescence at $\lambda_{ex/em}$ of 633/680–740 nm. Scale bars, 25 μm. (B, C) FL intensity in single cell area obtained from (A) with a Leica software. (D, E) *In vitro* casp-9 and casp-3 kit analysis of the cell extracts with the standard curves shown in (F) and (G). (H, I) Calibration curves for activity detection of intracellular casp-9 and casp-3.

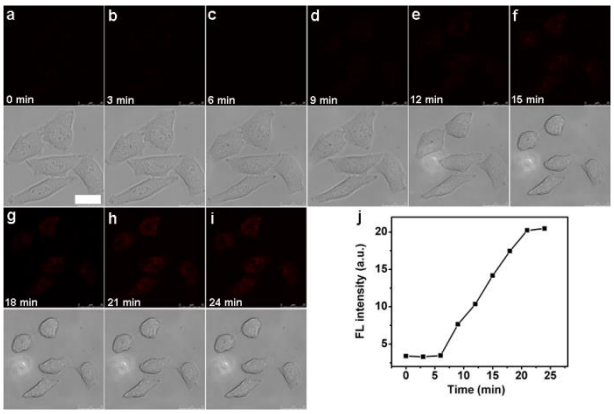

Fig. 8 Real-time monitoring of fluorescence and morphology of HeLa cells treated with nanoprobe (10 μL) for 3 h and then NIR irradiation at a power density of 4 W cm^{-2} for different times (a-i) at $\lambda_{ex/em}$ of 633/680–740 nm (top) and bright field (bottom). Scale bar, 25 μm. (j) Time course of fluorescence intensity obtained from the Leica software for a-i.

significantly inhibited at 24-h postirradiation (see ESI, Fig. S16†). The evaluation of excised tissues further demonstrated that the strong fluorescence occurred in the cancer tissue in comparison with the other organs such as liver and kidneys (see ESI, Fig. S17†), indicating the cleavage of peptide-9 and/or peptide-3 by corresponding active caspases. With the reduced tumor volume, the fluorescence acquired at both 680–800 nm for Cy5.5 (Fig. 9A) and 500–620 nm for FITC (Fig. 9B) from the irradiated tumor increased gradually after the laser irradiation. The more obvious background in Fig. 9B could be attributed to the auto-fluorescence at the excitation wavelength of 455 nm, which was greatly reduced under NIR excitation (Fig. 9A). Furthermore, the fluorescence of FITC for casp-9 showed earlier and greater change (Fig. 9B) than that of Cy5.5 for casp-3 (Fig. 9A), which indicated that casp-9 was activated prior to casp-3 and accorded with the above cellular experiments. As expected, the unirradiated mouse showed negligible change in the fluorescence (the left in Fig. 9A) and growing tumor volume. Therefore, the nanoprobe was efficient to *in situ* activate and monitor caspase family activity as the therapeutic feedback in living mice.

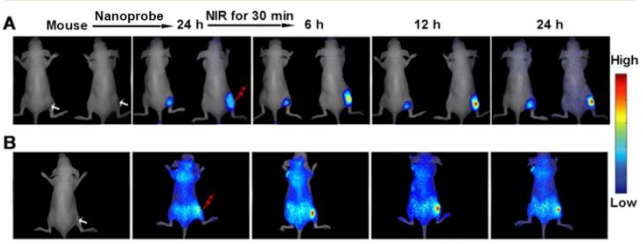

Fig. 9 *In vivo* monitoring the change of casp-3 (A) and casp-9 (B) activities on subcutaneous HeLa tumor-bearing mice after injection with the nanoprobe (100 μL) and irradiation with 808-nm laser for 30 min using left nanoprobe-injected mouse as control. (A) Excitation: 661 nm; emission: 680–800 nm. (B) Excitation: 455 nm; emission: 500–620 nm.

Conclusions

This work designs a protocol to *in situ* monitor the evolution of intracellular caspase from upstream to downstream activated by the nanocarrier with the therapeutical effect for inducing cell apoptosis. The evolution is performed by sequentially lighting up the fluorescence of dyes labelled to peptides assembled on the nanocarrier via caspase-catalytic cleavage. The fluorescence signal can be used for not only *in situ* quantification of both caspa-9 and casp-3 activities in cancer cells but also as a self-feedback of therapeutic response to cancer cells, which leads to a significant method for monitoring therapeutic effect *in vivo*. This methodology is applicable for other nanocarriers with the relative effect to monitor the caspase-dependent apoptosis. The strategy not only offers a new insight for real-time monitoring the evolution of intracellular caspase family and evaluating the therapeutic efficacy but also accelerates the uncovering of the biological roles of caspases in cancer apoptosis.

Acknowledgements

This study was supported by National Natural Science Foundation of China (21375060, 21135002, 21121091) and Priority development areas of The National Research Foundation for the Doctoral Program of Higher Education of China (20130091130005).

Notes and references

1 (a) J. F. Lovell, M. W. Chan, Q. C. Qi, J. Chen and G. Zheng, *J. Am. Chem. Soc.*, 2011, **133**, 18580–18582; (b) L. Yu, A. Alva, H. Su, P. Dutt, E. Freundt, S. Welsh, E. H. Baehrecken and M. J. Lenardo, *Science*, 2004, **304**, 1500–1502.

2 (a) G. M. Cohen, *Biochem. J.*, 1997, **326**, 1–16; (b) A. M. Hunter, E. C. LaCasse and R. G. Korneluk, *Apoptosis*, 2007, **12**, 1543–1568; (c) Y. G. Shi, *Protein Sci.*, 2004, **13**, 1979–1987.

3 (a) G. C. Van de Bittner, C. R. Bertozzi and C. J. Chang, *J. Am. Chem. Soc.*, 2013, **135**, 1783–1795; (b) E. M. Barnett, X. Zhang, D. Maxwell, Q. Chang and D. Piwnica-Worms, *Proc. Natl. Acad. Sci. U.S.A.*, 2009, **106**, 9391–9396; (c) H. B. Wang, Q. Zhang, X. Chu, T. T. Chen and J. Ge, R. Q. Yu, *Angew. Chem. Int. Ed.*, 2011, **50**, 7065–7069; (d) D. J. Ye, A. J. Shuhendler, L. N. Cui, L. Tong, S. S. Tee, G. Tikhomirov, D. W. Felsher and J. H. Rao, *Nat. Chem.*, 2014, **6**, 519–526; (e) M. Y. Hu, L. Li, H. Wu, Y. Su, P. Y. Yang, M. Uttamchandani, Q. H. Xu and S. Q. Yao, *J. Am. Chem. Soc.*, 2011, **133**, 12009–12020; (f) W. Gao, L. F. Ji, L. Li, G. W. Cui, K. H. Xu, P. Li and B. Tang, *Biomaterials*, 2012, **3**, 3710–3718.

4 (a) L. Zhu, X. L. Huang, K. Y. Choi, Y. Ma, F. Zhang, G. Liu, S. Lee and X. Y. Chen, *J. Control. Release*, 2012, **163**, 55–62; (b) X. L. Huang, M. Swierczewska, K. Y. Choi, L. Zhu, A. Bhirde and J. Park, *Angew. Chem. Int. Ed.*, 2012, **51**, 1625–1630.

5 (a) A. Kanno, Y. Yamanaka, H. Hirano, Y. Umezawa and T. Ozawa, *Angew. Chem. Int. Ed.*, 2007, **46**, 7595–7599; (b) N. Dai, J. Guo, Y. N. Teo and E. T. Kool, *Angew. Chem. Int. Ed.*, 2011, **50**, 5105–5109; (c) B. Shen, J. H. Jeon, M. Palner, D. J. Ye, A. Shuhendler, F. T. Chin and J. H. Rao, *Angew. Chem. Int. Ed.*, 2013, **52**, 10511–10514.

6 Y. Y. Yuan, R. T. K. Kwok, B. Z. Tang and B. Liu, *J. Am. Chem. Soc.*, 2014, **136**, 2546–2554.

7 (a) D. K. Yi, I. C. Sun, J. H. Ryu, H. Koo, C. W. Park, I. C. Youn, K. Choi, I. C. Kwon, K. Kim and C. H. Ahn, *Bioconjugate Chem.*, 2010, **21**, 2173–2177; (b) V. Shanmugam, S. Selvakumar and C. S. Yeh,

Chem. Soc. Rev., 2014, **43**, 6254–6287; (c) X. H. Huang, S. Neretina, and M. A. El-Sayed, *Adv. Mater*., 2009, **21**, 4880–4910; (d) W. A. Zhao and J. M. Karp, *Nat. Mater*., 2009, **8**, 453–454; f) P. K. Jain, X. H. Huang, I. H. El-Sayed and M. A. El-Sayed, *Acc. Chem. Res.*, 2008, **41**, 1578–1586.

8 (a) J. L. Li, D. Day and M. Gu, *Adv. Mater*., 2008, **20**, 3866–3871; (b) X. H. Huang, I. H. El-Sayed, W. Qian and M. A. El-Sayed, *J. Am. Chem. Soc*., 2006, **128**, 2115–2120.

9 H. W. Liao and J. H. Hafner, *Chem. Mater*., 2005, **17**, 4636–4641.

10 10 H. Jin, P. H. Yang, J. Y. Cai, J. H. Wang and M. Liu, *Appl. Microbiol. Biotechnol*., 2012, **94**, 1199–1208.

11 K. Boeneman, B. C. Mei, A. M. Dennis, G. Bao, J. R. Deschamps, H. Mattoussi and I. L. Medintz, *J. Am. Chem. Soc.*, 2009, **131**, 3828–3829.

12 H. B. Shi, R. T. K. Kwok, J. Z. Liu, B. G. Xing, B. Z. Tang and B. Liu, *J. Am. Chem. Soc*., 2012, **134**, 17972–17981.

13 (a) L. M. Wang, Y. Liu, W. Li, X. M. Jiang, Y. Ji, X. C. Wu, L. G. Xu, Y. Qiu, K. Zhao, T. T. Wei, Y. F. Li, Y. L. Zhao and C. Y. Chen, *Nano Lett*., 2011, **11**, 772–780; (b) L. Tong and J. X. Cheng, *Nanomedicine*, 2009, **4**, 265–276; (c) P. M. Kasili, J. M. Song and T. Vo-Dinh, *J. Am. Chem. Soc*., 2004, **126**, 2799–2806.

14 T. L. Deckwerth and E. M. Johnson, *J. Cell Biol*., 1993, **123**, 1207–1222.

15 I. Vermes, C. Haanen, H. Steffensnakken and C. Reutelingsperger, *J. Immunol. Methods*, 1995, **184**, 39–51.

Cite this: DOI: 10.1039/c0xx00000x

www.rsc.org/xxxxxx

ARTICLE TYPE

Table of contents

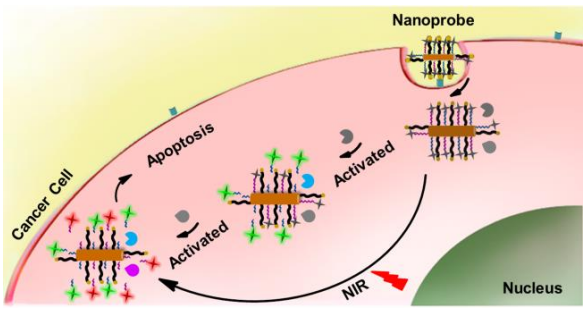

An intergrated nano-platform is designed to achieve in situ activation, monitoring and signal feedback of caspase family evolution.